GDCh

Research Articles

Angewandte
Chemie
International Edition
www.angewandte.org

Nanomotors   Hot Paper

Torque-Driven Orientation Motion of Chemotactic Colloidal Motors

Chang Zhou[+], Changyong Gao[+], Yingjie Wu,* Tieyan Si, Mingcheng Yang,* and Qiang He*

Abstract: *We report a direct experimental observation of the torque-driven active reorientation of glucose-fueled flasklike colloidal motors to a glucose gradient exhibiting a positive chemotaxis. These streamlined flasklike colloidal motors are prepared by combining a hydrothermal synthesis and a vacuum infusion and can be propelled by an enzymatic cascade reaction in the glucose fuel. Their flasklike architecture can be used to recognize their moving posture, and thus the dynamic glucose-gradient-induced alignment and orientation-dependent motility during positive chemotaxis can be examined experimentally. The chemotactic mechanism is that the enzymatic reactions inside lead to the glucose acid gradient and the glucose gradient which generate two phoretic torques at the bottom and the opening respectively, and thus continuously steer it to the glucose gradient. Such glucose-fueled flasklike colloidal motors resembling the chemotactic capability of living organisms hold considerable potential for engineering active delivery vehicles in response to specific chemical signals.*

Introduction

Directional migration and taxis play a vital role for the survival of biological systems. Chemotaxis refers to the directional locomotion of living organisms either toward or away from specific chemical stimuli. For instance, *Escherichia coli* (*E. coli*) can sense the gradient of nutrients (e.g., glucose) and swim toward the food-rich area.[1–3] Inspired by biologically chemotactic behaviors, a variety of chemically-powered colloidal motors with a positive or negative chemotaxis have been developed.[4–10] In particular, the small size

[*]   C. Zhou,[+] Dr. C. Gao,[+] Dr. Y. Wu, Dr. T. Si, Prof. Q. He
      Key Laboratory of Microsystems and Microstructures Manufacturing (Ministry of Education), School of Medicine and Health
      Harbin Institute of Technology
      No. 92 XiDaZhi Street, Harbin, 150001 (China)
      E-mail: yingjiewu@hit.edu.cn
              qianghe@hit.edu.cn

      Prof. M. Yang
      Beijing National Laboratory for Condensed Matter Physics and
      Laboratory of Soft Matter Physics, Institute of Physics
      Chinese Academy of Sciences, Beijing, 100190 (China)
      and
      School of Physical Sciences, University of Chinese Academy of
      Sciences, Beijing 100049 (China)
      and
      Songshan Lake Materials Laboratory
      Dongguan, Guangdong 523808 (China)
      E-mail: mcyang@iphy.ac.cn

[+]   These authors contributed equally to this work.

and self-propulsion capability of these synthetic colloidal motors enable them to bring revolutionary solutions for future precision-medicine applications such as active target delivery,[11–18] microsurgery,[19,20] nanoscale assembly[21–23] and nanorobotics.[24–30] The unguided chemically-propelled colloidal motors only exhibit an enhanced Brownian diffusion on large timescales, and obviously it is crucial to achieve directional control over motion for practical applications.

It has been reported that the synthesized colloidal motors powered by chemical/biochemical reactions can autonomously migrate toward the region with a higher or lower concentration of chemical fuels.[23,31–40] Note that the proposed mechanisms in these reports are significantly different since these so-called chemotactic behavior is based upon a statistical result of many colloidal motors rather than direct observation of individuals. Recently, theoretical analysis and numerical simulation suggest that the chemotaxis of Janus spherical colloidal motors should mainly originate from the alignment of Janus colloidal motors with the chemical gradient and the orientation-dependent motility like a physical mechanism of biological chemotaxis found in nature.[41,42] More recently, Guan et al. experimentally demonstrate the self-reorientation-induced biomimetic chemotaxis which is generated by the difference of chemical reaction rates across the surface of a Janus ZnO-based spherical micromotor.[43] These theoretical prediction and experimental results greatly advance our understanding of the chemotaxis of artificial motors. When the size of spherical colloidal motors is down to sub-micrometer scales, however, they are continuously reoriented by the collisions of solvent molecules in the fluid, i.e. a strong Brownian force, which leads to a weak chemotactic capability or a random diffusional process. Nevertheless, engineering a new type of bio-friendly, sub-micrometer-sized colloidal motors with an identifi-able moving posture and a strong chemotaxis is still highly requested for both the underlying chemotactic mechanism and future biomedical application.

Herein, we present the design of a glucose-fueled flasklike colloidal motor based on a hydrothermal synthesis and experimentally investigate the torque-driven active alignment and reorientation-dependent motility of these colloidal motors during chemotactic motion. The streamlined flasklike colloidal motors have a reduced fluid-resistance coefficient and can autonomously move due to the cascade reaction of glucose oxidase (GOx) and catalase (Cat) occurring in the flask cavity. The difference in diffusion rates across the surface of the flasklike colloidal motor can make a phoretic torque that uninterruptedly directs it into the gradient of glucose fuel. It can counteract the orientation effect by solvent molecule collisions, and thus the opening

can rotate toward the glucose gradient field, realizing a chemotactic motion.

Results and Discussion

The sub-micrometer-sized, streamlined and glucose-fueled flasklike colloidal motors were synthesized by combining a hydrothermal synthesis and a vacuum infusion as schematically illustrated in Figure 1A according to previously reported procedures.[44,45] Briefly, the mixed micelles containing double surfactants P123 and oleic acid form nanoemulsions in a hydrothermal environment. The polymerization of the ribose molecules occurs on the surface of nanoemulsions. With the increasing reaction time, the resulting polymer shell increasingly expands, and then ruptures to form the hollow flasklike particles. Next, the as-prepared flasklike particles were added into the phosphate buffer saline (PBS) solution containing both GOx and Cat under a vacuum condition so that two enzymes could be loaded into the inner cavity. The scanning electron microscopy (SEM) image shows that the synthesized colloidal motors have a well-defined round-bottom flasklike structure (Figure S1). The length of the colloidal motors is 850 ± 45 nm whereas the outside diameters of the neck and the spherical bottom are 350 ± 53 and 700 ± 32 nm, respectively.
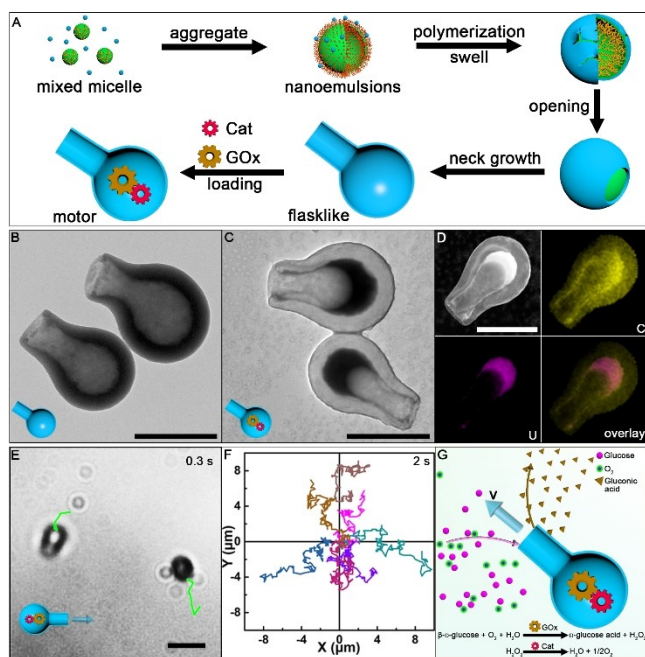
Figure 1. Preparation and self-propelled motion of the glucose-fueled round-bottom flasklike colloidal motors. A) Scheme of the synthesis of the hydrophilic flasklike motors. TEM images of the flasklike colloidal particles (B) and the flasklike colloidal motors (C). D) STEM and corresponding TEM-mapping images of the elemental distribution of carbon and uranium. Scale bar, 500 nm. E) Optical image of the autonomous motion of flasklike colloidal motors in 100 mM glucose solution in 0.3 s. Scale bar, 1 μm. F) Corresponding trajectories of six glucose-fueled flasklike colloidal motors in 2 s. G) Schematic illustration of the reaction occurring in colloidal motors.

The transmission electron microscopy (TEM) image (Figure 1B) displays the hollow cavity inside the round bottom, a single opening at the end of neck and a straight channel. The inside diameter of the channel is 200 ± 53 nm at minimum and the inner diameter of the cavities are 550 ± 33 nm, which provides prerequisites for the loading cargoes such as enzymes. The positively staining TEM image (Figure 1C) shows the black regions in the inner cavity, representing the enzymes stained with uranyl acetate. Figure 1D shows the distribution of GOx and Cat inside the cavity of the flasklike colloidal motors analyzed by the scanning transmission electron microscopy (STEM) coupled with energy dispersive X-ray (EDX) elemental mapping. Besides, the contact angle of $58 \pm 4°$ confirms the hydrophilicity of as-prepared flasklike colloidal motors (Figure S2), which is highly related to the direction of the self-propulsion as previously studied.[44] The time-lapse optical image in Figure 1E (see also Video S1 in Supporting Information) shows the self-propelled motion of as-prepared flasklike colloidal motors at a speed of $3.15\ \mu m\,s^{-1}$ in 100 mM glucose solution along a direction from the round-bottom to the opening. Figure 1F shows the typical trajectories of six flasklike colloidal motors self-propelled without specified direction in the absence of glucose gradient. Figure 1G shows the schematic illustration of the enzymatic cascade reaction occurring in the flasklike colloidal motors, which mainly forms the glucose and gluconic acid gradients around the opening of flasklike colloidal motors. As studied in the previous work,[44] the competition of the generated local glucose gradient and gluconic acid gradient provides the net driving force to propel the flasklike colloidal motors. Given that the driving force generated from the glucose gradient is larger than the opposite force by the gluconic acid gradient, the hydrophilic flasklike colloidal motors thus move with opening forward, in agreement with the experimental observation in Figure 1E.

To examine whether these hydrophilic flasklike colloidal motors exhibit a chemotactic motion, a cylindrical agarose gel presoaked in 1 M glucose solution overnight was placed on the right edge of the PBS solution-filled petri dish to establish the glucose gradient (Figure 2A). Figure S3 shows the simulated glucose distribution in the petri dish after 1 h. The glucose gradually diffuses from the agarose gel in the form of concentric circles, and the glucose concentration decreases with the increasing distance from the agarose gel. When the glucose gradient was established, the flasklike colloidal motors were injected in the middle of the petri dish. The time lapse images of flasklike colloidal motors in Figure 2B (see also Video S2 in Supporting Information) show that these motors could sense the local glucose gradient, align and move along the glucose gradient toward the glucose-rich areas (i.e. positive chemotaxis) accompanying with a continuous reorientation. To better examine the reorientation process of flasklike colloidal motors, the trajectories of flasklike colloidal motors responding to the glucose gradient was tracked as illustrated in Figure 2C. Obviously, the normalized trajectories of flasklike colloidal motors are biased toward the source of glucose, representing a positive chemotaxis. As a control, when the agarose gel
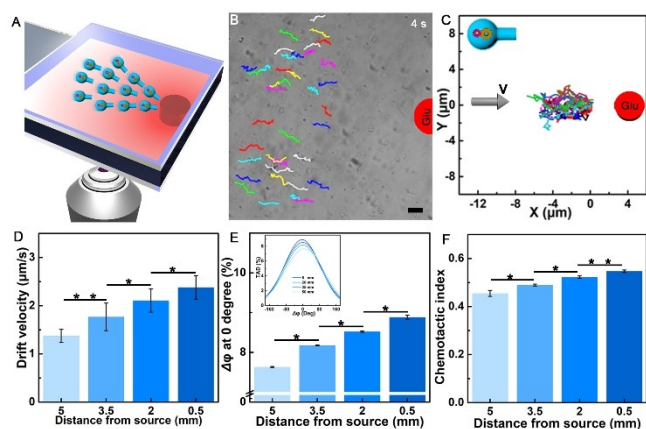
Figure 2. Observation and analysis of the chemotaxis of flasklike colloidal motors in the PBS solution. A) Scheme of the device for chemotaxis. B) Time lapse images of the chemotaxis of the flasklike colloidal motors. Scale bar, 5 μm. C) Corresponding track trajectories of chemotaxis of the flasklike colloidal motors in 4 s. D) Drift velocity of flasklike colloidal motors at different distances from the glucose source. E) Turning angle distribution (TAD) at 0 degree of the flasklike colloidal motors at different distances from the glucose source. Inset: TAD distribution. F) Chemotactic index (CI) of the flasklike colloidal motors at different distances from the glucose source. * Denotes the significant difference ($*P < 0.05$, $**P < 0.01$). Each data point was acquired by statistically analysing at least 40 flasklike colloidal motors (D, E and F).

containing glucose was replaced by that only containing PBS, the flasklike colloidal motors exhibit typical Fickian diffusion profile with stochastic trajectories (Figure S4, see also Video S3 in Supporting Information). In a control, the agarose gel containing glucose was placed on different sites of the used petri dish. The time lapse images in Figure S5 (see also Video S4 and S5 in Supporting Information) and normalized trajectories demonstrate the device asymmetry is irrelevant to the directional motion of flasklike colloidal motors toward the source of glucose. Furthermore, when the flasklike colloidal particles without enzymes were added, they moved away from the agarose gel containing glucose due to the diffusiophoretic force generated by the glucose gradient (Figure S6, see also Video S6 in Supporting Information).

In addition to the trajectory analysis, the average drift velocity was measured according to the projection of actual velocity on the glucose gradient. Figure 2D shows that the average drift velocity of flasklike colloidal motors increases from $1.37 \pm 0.33 \, \mu m \, s^{-1}$ at 5 mm from the source to $2.37 \pm 0.54 \, \mu m \, s^{-1}$ at 0.5 mm, demonstrating that the flasklike colloidal motors become more chemotactic in the case of approaching the source of glucose. To gain insight into the biased motion toward the glucose source, the turning angle distribution (TAD) of flasklike colloidal motors was introduced by measuring the angle of displacement with respect to the previous step at the same time interval, which is defined $\Delta\phi$ as schematically illustrated in Figure S7. Figure 2E shows the TAD at 0 degree of the flasklike colloidal motors significantly increases when approaching the glucose source, indicating the enhancing chemotactic capacity to-

ward the glucose source. The inset illustrates that the TAD is polarized along the direction of glucose gradient. Also, the migration persistence was further analyzed by the chemotactic index (CI) which was calculated as the ratio of the displacement to the total migration path length.[46,47] Figure 2F shows that the value of CI is dependent on the distance from the glucose source, suggesting that the higher glucose gradient results in the stronger directional migration. Taken together, the directional migration ability of flasklike colloidal motors is strongly biased by the self-reorientation of flasklike colloidal motors in the glucose gradient, and the diffusiophoretic force generated by the glucose gradient field is negligible. Hence, the flasklike colloidal motors can create a higher asymmetry angular probability and continuously direct it to the glucose gradient.

To further elucidate the chemotactic behaviour, the kinematic behaviour of flasklike colloidal motors in the chemotactic process was examined under an optical microscopy equipped with a high-resolution CCD camera owing to their distinct flask-shaped structure. To better record the flasklike architecture, the PBS was replaced by the mixture of PBS and glycerol (7:3) because the increased viscosity can reduce the Brownian rotation. The time lapse images in Figure 3A (see also Video S7 in Supporting Information) and correspondingly schematic illustration in Figure 3B display that the flasklike colloidal motor dynamically rotated the opening toward the source of glucose when it deviated the gradient due to the perturbation of a strong Brownian force. Based on the above observation, we quantitatively analysed the orientational angle $|\Delta\theta|$ between the polarity of the flasklike colloidal motor (black arrow) and the direction of glucose gradient (red arrow) with time evolution in the self-reorientation process (Figure 3C). It reveals that the orientational motion of the flasklike colloidal motor is highly correlated to the glucose gradient. Figure 3D shows that the orientational angle $|\Delta\theta|$ at different distances from the source mainly distributed below 90°, indicating that the vector of the flasklike colloidal motor dynamically reorientated toward the gradient. More interestingly, the asymmetric distribution of the flasklike colloidal motor becomes more distinct with the decreasing distance from the glucose source, which reflects that higher glucose gradient can increase the chemotactic ability of the flasklike colloidal motor. Note that the increased distribution of the orientational angle $|\Delta\theta|$ below 90° is inversely proportional to the distances from the glucose source, indicating that they can take less time reorienting the vector toward the gradient closer to the source. Figure 3E shows the drift velocity as a function of the orientational angle $|\Delta\theta|$ of the flasklike colloidal motor. When the opening points to the source of glucose ($|\Delta\theta| < 90°$), the flasklike colloidal motor swims toward the source with a positive velocity. When the opening is against the glucose gradient ($|\Delta\theta| > 90°$), however, the negative drift velocity reflects the influence of the Brownian force and the glucose gradient field force on the rotation process of flasklike colloidal motors. Note that the area by the plotted curve at $|\Delta\theta| < 90°$ is clearly larger
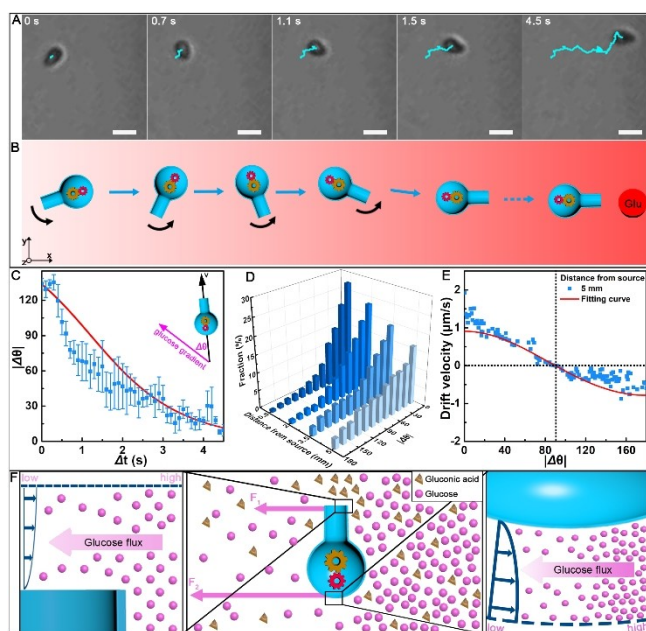
Figure 3. Direct observation of the self-reorientation of the flasklike colloidal motor in the chemotaxis toward the source of glucose in the mixture of PBS solution and glycerol (7:3). A) Time lapse images of the dynamic rotation of the flasklike colloidal motor to the glucose gradient. Scale bar, 1 μm. B) Correspondingly schematic illustration in A. C) Orientational angle $|\Delta\theta|$ evolution of the flasklike colloidal motors as a function of Δt in the chemotaxis. The blue symbols represent the experimental data and the red line refers to the predicted curve from Equation (6). Inset, black arrow: the orientational vector of the flasklike colloidal motor; red arrow: the direction of the glucose gradient. D) The distribution of the orientational angle $|\Delta\theta|$ of the flasklike colloidal motors at different distances from the source of glucose. E) The drift velocity as a function of orientational angle $|\Delta\theta|$ of the flasklike colloidal motors derived from 5 mm from the source of glucose. The blue symbol and the red line refer to the experimental data and the fitting curve with Equation (1), respectively. F) Scheme of the mechanism of the reorientation of the flasklike colloidal motor in the chemotaxis. Each data point was obtained from at least 10 flasklike colloidal motors (C, D and E).

than that at $|\Delta\theta| > 90°$, indicating the self-propelling speed is anisotropic.

As schematically illustrated in Figure 3F, from a molecular point of view, the glucose concentration gradients produce the diffusiophoretic force F_1 on the opening and the diffusiophoretic force F_2 on the round bottom, respectively. Note that the gluconic acids generated by the enzymatic cascade reactions occurring in the cavity dilute the glucose gradient around the opening. The difference value of two diffusiophoretic forces $(F_2 - F_1)$ generated by the nonsymmetric local concentration gradients of different chemical species results in a net self-diffusiophoretic torque exerting on the flasklike colloidal motors. As a consequence, this self-diffusiophoretic torque $(F_2 - F_1 > 0)$ can counteract the effect by the molecular collisions in fluid, which makes the opening to rotate toward the direction of the glucose gradient field, and finally achieve a positively chemotactic motion. The microscopically chemotactic mechanism of the flasklike colloidal motors is different with the natural

bacteria such as *E. coli.* The latter exhibits a "run-and-tumble" motion behavior in the chemotaxis through their self-reorientation based on the spatial comparison of chemical signal intensity and a biased random walk toward the glucose source (Figure S8).[48] However, the torque-driven reorientation motion of the chemotactic flasklike colloidal motors may still mimic the self-reorientation behavior of *E. coli* in the positive chemotaxis.

To reveal the underlying mechanism, a quantitative description is presented based on a minimal model. Since the source of glucose is a cylindrical agarose gel, the steady-state glucose flux is inversely proportional to the distance from the source center $j \propto r^{-1}$ due to the mass continuity and Fick's law. Neglecting the convection, the glucose concentration profile is thus $c(r) = c_0 - c_1 \ln(r)$, with c_0 and c_1 the unknown coefficients, which can be determined by the boundary conditions. For a point-like motor in the chemical gradient, its self-propelling velocity is proportional to the local fuel concentration at the motor position, $v_s(r) = v_0 - v_1 \ln(r) \propto c(r)$. The flasklike colloidal motor has a finite size, however, its self-propulsion velocity should depend on the motor orientation, as the effective fuel concentration felt by the opening of the flasklike colloidal motors is orientation-dependent when the motor center remains the same. The maximum and minimum self-propulsion velocity correspond to the situations of the opening toward and against the fuel source, respectively. Moreover, the anisotropic degree of the self-propelling velocity increases with the increasing local chemical gradient, $\nabla c(r) \propto r^{-1}$. Thus, it is reasonable to take the self-propelling velocity as:

$$v_s(r, \theta) = [v_0 - v_1 \ln(r)](1 + r^{-1}\delta\cos\theta) \qquad (1)$$

with θ the angle of the motor opening with respect to the glucose source. Here, the free parameters v_0, v_1 and δ are determined by using Equation (1) to fit the experimental data of the drift velocity $v_s(r,\theta)\cos\theta$ in the 30 % glycerol solution (Figure 3E). With the same values of the fitting parameters (given in Table 1), Equation (1) can well fit the drift velocity-θ curves for different distances, as demonstrated in Figure 3E (and Figure S9 in Supporting Information).

As mentioned in Figure 3F, two self-diffusiophoretic forces in the glucose gradient generate a phoretic torque to rotate the flasklike colloidal motor. Clearly, this torque is proportional to the local chemical gradients and also depends on the motor orientation with the maximum magnitude at $\theta = \pm\pi/2$ and the vanishing magnitude at

Table 1: The free parameters in Equations (1) and (2) for the flasklike colloidal motors in the 30 % glycerol solution are extracted by fitting Equations (1) and (3) to the corresponding experimental data. All the parameters are expressed in International System of units (SI units).

	v_0	v_1	δ	$\beta\tau_0$
flasklike colloidal motor	4.6×10^{-7}	7.4×10^{-8}	4×10^{-4}	3.41×10^{-3}

$\theta = 0, \pi$. Similarly, the phoretic torque is reasonably taken as

$$\tau(r, \theta) = -\tau_0 r^{-1} \sin\theta \qquad (2)$$

with τ_0 the fitting prefactor. We relate the torque to an effective angle potential, $U(r, \theta) = -\tau_0 r^{-1} \cos\theta$, and further assume that the motor orientation approximately obeys an equilibrium probability distribution,

$$P(r, \theta) \propto \exp(\beta\tau_0 r^{-1}\cos\theta) \qquad (3)$$

with $\beta = 1/k_B T$ (T the temperature). Equation (3) can be well fitted to the experimental data in Figure 4A (and Figure S10 in Supporting Information), which yields the free parameter τ_0, as provided in Table 1. These extracted free parameters can be then used as input quantities of Equations (1) and (2) for performing the following simulations and theoretical calculations.

Firstly, we performed the Brownian dynamics simulations to reproduce the chemotaxis of the colloidal motor. Because of the system symmetry, the flasklike colloidal motor is modelled as a two-dimensional active particle experiencing a self-propelling velocity and a phoretic torque. In simulations, the translational dynamics of the colloidal motor is updated according to overdamped Langevin equation,

$$\gamma\boldsymbol{v} = v_s\boldsymbol{n} + \xi \qquad (4)$$

where γ is the translational friction coefficient, $\boldsymbol{n}$ the unit vector of the motor symmetric axis (from the round bottom to the opening), the self-propelling velocity v_s is described by Equation (1), and ξ refers to the Gaussian-distributed stochastic force with zero mean and variance $\langle\xi_\alpha(t)\xi_\beta(t')\rangle = 2k_B T\gamma\delta_{\alpha\beta}\delta(t - t')$ with α and β Cartesian components. The orientational evolution of the flasklike colloidal motor is similarly described by

$$\gamma_r\omega = \tau + \xi_r \qquad (5)$$

with γ_r the rotational friction coefficient, ω the angular velocity, τ the phoretic torque described by Equation (2), and the Gaussian stochastic torque ξ_r possessing the variance $\langle\xi_{r\alpha}(t)\xi_{r\beta}(t')\rangle = 2k_B T\gamma_r\delta_{\alpha\beta}\delta(t - t')$. For simplicity, the frictional coefficients γ and γ_r are estimated by approximating the flasklike colloidal motor as a spherical-shell particle of outer diameter 0.7 μm and inner diameter 0.55 μm. Substituting the parameters given in Table 1 into Equations (4) and (5), the simulations are implemented to collect the particle trajectories, as shown in Figure 4B. The resulting simulation results clearly show a positively chemotactic behavior.
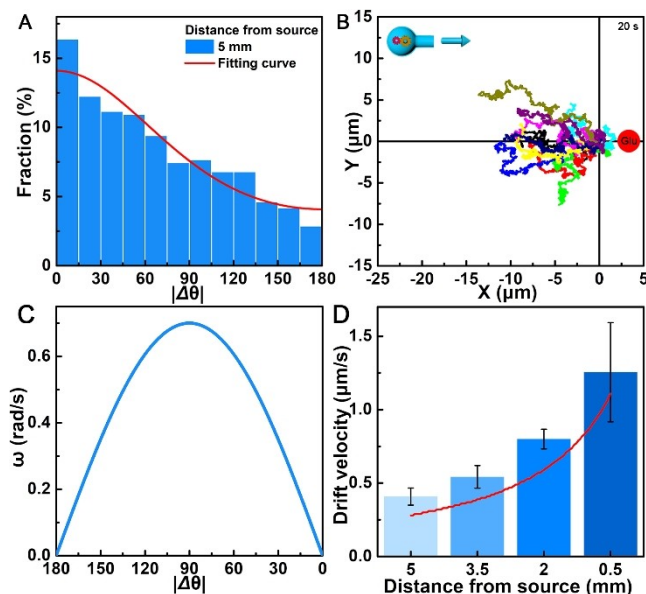
Secondly, we use Equations (1)–(3) and the extracted parameters to theoretically calculate the orientational angle evolution and drift velocity of the colloidal motor. Combining Equation (2) and the mean torque balance condition $\gamma_r\omega = \tau$, we can derive the time evolution of the motor orientational angle

$$t = \omega_0^{-1}\ln[(\csc\theta - \cot\theta)/(\csc\theta_0 - \cot\theta_0)], \qquad (6)$$

with θ_0 the orientational angle at $t = 0$, and $\omega_0 = -\tau_0 r^{-1}\gamma_r^{-1}$ the rotational velocity of the motor at $\theta = \pi/2$. Inserting the known quantity τ_0 into Equation (6) yields the evolution of θ, which is well consistent with the experimental data in Figure 3C without free parameter. From Equation (6), the turning rate and phoretic torque of the motor are straightforwardly calculated, as shown in Figure 4C and S11. Further, based on Equations (1) and (3), the r-dependence of the drift velocity of the colloidal motor can be easily calculated by integrating out the orientational angle, $\int_0^{2\pi} P(r, \theta)v_s(r, \theta)\cos\theta d\theta$. The theoretical prediction reproduces the experimental measurement, as shown in Figure 4D. The good agreement between the theoretical predictions and experimental results indicates that our minimal model properly captures the essential mechanism underlying the chemotaxis of the flasklike colloidal motor.

Figure 4. A) The distribution of the orientational angle $|\Delta\theta|$ of the flasklike colloidal motors in the chemotaxis at 5 mm from the source in the mixture of PBS solution and glycerol (7:3). Red line is the fitting curve with Equation (3). B) Simulated track trajectories of the positive chemotaxis of the flasklike colloidal motors in the mixture of PBS solution and glycerol (7:3). C) The turning rate as a function of the orientational angle $|\Delta\theta|$ of the flasklike colloidal motors in the chemotaxis predicted based on Equation (6). D) The distribution of the drift velocity in the mixture of PBS solution and glycerol (7:3) as a function of the distance from the glucose source. Red line is the drift velocity predicted based on the minimal theoretical model.

Conclusion

We have demonstrated a positive chemotaxis of the sub-micrometer-sized, streamlined and glucose-fueled flasklike colloidal motors along a glucose concentration gradient resembling that of the chemotactic microorganisms in

nature. Benefiting from their unique round-bottomed flask-like architecture, the change of moving postures of these sub-micrometer-sized colloidal motors could be experimentally recorded under an optical microscopy. Direct kinematic analysis reveals the dynamic glucose-gradient-induced alignment and the phoretically torque-driven active reorientation of glucose-fueled flasklike colloidal motors. The microscopic mechanism of the chemotactic flasklike colloidal motors is that the nonsymmetric local concentration gradients of different chemical species by the enzymatic cascade reactions results in a net self-diffusiophoretic torque on the flasklike colloidal motors. Accordingly, the self-diffusiophoretic torque continuously steers them to the glucose concentration gradient and thus achieve a positive chemotaxis motion. The subsequent calculations and theoretical simulations further verify the microscopic mechanism of the chemotactic flasklike colloidal motors. These sub-micrometer-sized, streamlined and glucose-fueled flasklike colloidal motors with a strong chemotactic capacity may not only provide direct experimental evidence for the existing theoretical speculation, but also serve for active target delivery because of its small size, fuel biocompatibility and high loading volume.

Acknowledgements

Conflict of Interest

The authors declare no conflict of interest.

Data Availability Statement

The data that support the findings of this study are available on request from the corresponding author. The data are not publicly available due to privacy or ethical restrictions.

Keywords: Chemotaxis · Colloidal Motors · Enzymatic Cascade · Nanomotors · Self-Propulsion

[1] U. Alon, M. G. Surette, N. Barkai, S. Leibler, *Nature* **1999**, *397*, 168–171.

[2] Y. V. Kalinin, L. Jiang, Y. Tu, M. Wu, *Biophys. J.* **2009**, *96*, 2439–2448.

[3] R. Colin, K. Drescher, V. Sourjik, *Nat. Commun.* **2019**, *10*, 5329.

[4] D. A. Wilson, R. J. M. Nolte, J. C. M. van Hest, *Nat. Chem.* **2012**, *4*, 268–274.

[5] B. J. Toebes, F. Cao, D. A. Wilson, *Nat. Commun.* **2019**, *10*, 5308.

[6] X. Arqué, A. Romero-Rivera, F. Feixas, T. Patiño, S. Osuna, S. Sánchez, *Nat. Commun.* **2019**, *10*, 2826.

[7] X. Ma, A. C. Hortelao, A. Miguel-López, S. Sánchez, *J. Am. Chem. Soc.* **2016**, *138*, 13782–13785.

[8] S. Tang, F. Zhang, H. Gong, F. Wei, J. Zhuang, E. Karshalev, B. Esteban-Fernández de Ávila, C. Huang, Z. Zhou, Z. Li, L. Yin, H. Dong, R. H. Fang, X. Zhang, L. Zhang, J. Wang, *Sci. Robot.* **2020**, *5*, eaba6137.

[9] L. Kong, C. C. Mayorga-Martinez, J. Guan, M. Pumera, *Chem. Asian J.* **2019**, *14*, 2456–2459.

[10] Y. Xing, M. Zhou, T. Xu, S. Tang, Y. Fu, X. Du, L. Su, Y. Wen, X. Zhang, T. Ma, *Angew. Chem. Int. Ed.* **2020**, *59*, 14368–14372; *Angew. Chem.* **2020**, *132*, 14474–14478.

[11] B. E.-F. de Ávila, P. Angsantikul, J. Li, M. Angel Lopez-Ramirez, D. E. Ramírez-Herrera, S. Thamphiwatana, C. Chen, J. Delezuk, R. Samakapiruk, V. Ramez, M. Obonyo, L. Zhang, J. Wang, *Nat. Commun.* **2017**, *8*, 272.

[12] Y. Tu, F. Peng, A. A. M. André, Y. Men, M. Srinivas, D. A. Wilson, *ACS Nano* **2017**, *11*, 1957–1963.

[13] H. Zhang, Z. Cao, Q. Zhang, J. Xu, S. L. J. Yun, K. Liang, Z. Gu, *Small* **2020**, *16*, 2002732.

[14] A. C. Hortelão, T. Patiño, A. Perez-Jiménez, À. Blanco, S. Sánchez, *Adv. Funct. Mater.* **2018**, *28*, 1705086.

[15] M. Xuan, J. Shao, X. Lin, L. Dai, Q. He, *ChemPhysChem* **2014**, *15*, 2255–2260.

[16] M. Luo, Y. Feng, T. Wang, J. Guan, *Adv. Funct. Mater.* **2018**, *28*, 1706100.

[17] Y. Xing, M. Zhou, X. Du, X. Li, J. Li, T. Xu, X. Zhang, *Appl. Mater. Today* **2019**, *17*, 85–91.

[18] M. Xuan, J. Shao, J. Zhao, Q. Li, L. Dai, J. Li, *Angew. Chem. Int. Ed.* **2018**, *57*, 6049–6053; *Angew. Chem.* **2018**, *130*, 6157–6161.

[19] J. Vyskočil, C. C. Mayorga-Martinez, E. Jablonská, F. Novotný, T. Ruml, M. Pumera, *ACS Nano* **2020**, *14*, 8247–8256.

[20] M. Zhou, Y. Xing, X. Li, X. Du, T. Xu, X. Zhang, *Small* **2020**, *16*, 2003834.

[21] Y. Jia, J. Li, *Acc. Chem. Res.* **2019**, *52*, 1623–1631.

[22] J. Grauer, F. Schmidt, J. Pineda, B. Midtvedt, H. Löwen, G. Volpe, B. Liebchen, *Nat. Commun.* **2021**, *12*, 6005.

[23] B. Liebchen, A. K. Mukhopadhyay, *J. Phys. Condens. Matter* **2022**, *34*, 083002.

[24] T. G. Leong, C. L. Randall, B. R. Benson, N. Bassik, G. M. Stern, D. H. Gracias, *Proc. Natl. Acad. Sci. USA* **2009**, *106*, 703–708.

[25] G. Chatzipirpiridis, O. Ergeneman, J. Pokki, F. Ullrich, S. Fusco, J. A. Ortega, K. M. Sivaraman, B. J. Nelson, S. Pané, *Adv. Healthcare Mater.* **2015**, *4*, 209–214.

[26] D. Kagan, M. J. Benchimol, J. C. Claussen, E. Chuluun-Erdene, S. Esener, J. Wang, *Angew. Chem. Int. Ed.* **2012**, *51*, 7519–7522; *Angew. Chem.* **2012**, *124*, 7637–7640.

[27] A. A. Solovev, W. Xi, D. H. Gracias, S. M. Harazim, C. Deneke, S. Sanchez, O. G. Schmidt, *ACS Nano* **2012**, *6*, 1751–1756.

[28] S. K. Srivastava, M. Medina-Sánchez, B. Koch, O. G. Schmidt, *Adv. Mater.* **2016**, *28*, 832–837.

[29] S. Cao, J. Shao, H. Wu, S. Song, M. T. De Martino, I. A. B. Pijpers, H. Friedrich, L. K. E. A. Abdelmohsen, D. S. Williams, J. C. M. van Hest, *Nat. Commun.* **2021**, *12*, 2077.

[30] Y. Xing, X. Du, T. Xu, X. Zhang, *Soft Matter* **2020**, *16*, 9553–9558.

[31] C. Jin, C. Krüger, C. C. Maass, *Proc. Natl. Acad. Sci. USA* **2017**, *114*, 5089–5094.

[32] L. Baraban, S. M. Harazim, S. Sanchez, O. G. Schmidt, *Angew. Chem. Int. Ed.* **2013**, *52*, 5552–5556; *Angew. Chem.* **2013**, *125*, 5662–5666.

[33] A. Joseph, C. Contini, D. Cecchin, S. Nyberg, L. Ruiz-Perez, J. Gaitzsch, G. Fullstone, X. Tian, J. Azizi, J. Preston, G. Volpe, G. Battaglia, *Sci. Adv.* **2017**, *3*, e1700362.

Angew. Chem. Int. Ed. **2022**, e202116013 (6 of 7)

© 2022 Wiley-VCH GmbH

[34] F. Peng, Y. Tu, J. Hest, D. Wilson, *Angew. Chem. Int. Ed.* **2015**, *54*, 11662–11665; *Angew. Chem.* **2015**, *127*, 11828–11831.

[35] A. R. Morgan, A. B. Dawson, H. S. McKenzie, T. S. Skelhon, R. Beanland, H. P. W. Franks, S. A. F. Bon, *Mater. Horiz.* **2014**, *1*, 65–68.

[36] C. Chen, X. Chang, P. Angsantikul, J. Li, B. Esteban-Fernández de Ávila, E. Karshalev, W. Liu, F. Mou, S. He, R. Castillo, Y. Liang, J. Guan, L. Zhang, J. Wang, *Adv. Biosyst.* **2018**, *2*, 1700160.

[37] J. Plutnar, M. Pumera, *Angew. Chem. Int. Ed.* **2019**, *58*, 2190–2196; *Angew. Chem.* **2019**, *131*, 2212–2218.

[38] J. Zhuang, B.-W. Park, M. Sitti, *Adv. Sci.* **2017**, *4*, 1700109.

[39] A. Somasundar, S. Ghosh, F. Mohajerani, L. N. Massenburg, T. Yang, P. S. Cremer, D. Velegol, A. Sen, *Nat. Nanotechnol.* **2019**, *14*, 1129–1134.

[40] Y. Hong, N. M. K. Blackman, N. D. Kopp, A. Sen, D. Velegol, *Phys. Rev. Lett.* **2007**, *99*, 178103.

[41] M. N. Popescu, W. E. Uspal, C. Bechinger, P. Fischer, *Nano Lett.* **2018**, *18*, 5345–5349.

[42] B. Liebchen, H. Löwen, *Acc. Chem. Res.* **2018**, *51*, 2982–2990.

[43] F. Mou, Q. Xie, J. Liu, S. Che, L. Bahmane, M. You, J. Guan, *Natl. Sci. Rev.* **2021**, *8*, nwab066.

[44] C. Gao, C. Zhou, Z. Lin, M. Yang, Q. He, *ACS Nano* **2019**, *13*, 12758–12766.

[45] C. Chen, H. Wang, C. Han, J. Deng, J. Wang, M. Li, M. Tang, H. Jin, Y. Wang, *J. Am. Chem. Soc.* **2017**, *139*, 2657–2663.

[46] X. M. O'Brien, A. J. Loosley, K. E. Oakley, J. X. Tang, J. S. Reichner, *J. Leukocyte Biol.* **2014**, *95*, 993–1004.

[47] J. Shao, M. Xuan, H. Zhang, X. Lin, Z. Wu, Q. He, *Angew. Chem. Int. Ed.* **2017**, *56*, 12935–12939; *Angew. Chem.* **2017**, *129*, 13115–13119.

[48] V. Sourjik, N. S. Wingreen, *Curr. Opin. Cell Biol.* **2012**, *24*, 262–268.

Research Articles

C. Zhou, C. Gao, Y. Wu,* T. Si, M. Yang,*
Q. He* —————————— e202116013

Torque-Driven Orientation Motion of Che-
motactic Colloidal Motors
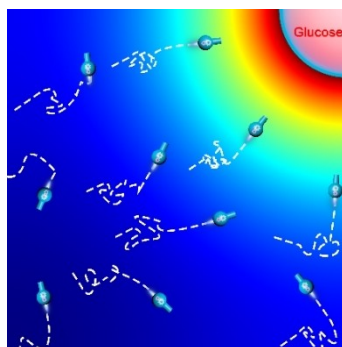
Enzymatic cascade reactions occurring
in the cavity of flasklike colloidal motors
have been shown to lead to the con-
sumption of the glucose fuel and a
decreased glucose concentration gra-
dient at the opening. The resulting
imbalance of self-diffusiophoretic forces
generates a phoretic torque on the flask-
like colloidal motors, which continuously
steers them to the glucose concentra-
tion gradient and thus results in a
positive chemotaxis motion